Available online at www.sciencedirect.com
ScienceDirect
Trans. Nonferrous Met. Soc. China 32(2022) 1217−1225
Transactions of Nonferrous Metals Society of China
www.tnmsc.cn

Effect of graphene on microstructure and properties of Gr/CuCr10 composites

Jin-feng LENG[1], Qing-bo ZHOU[2], Zhan-zhi LI[3], Yun-fan DONG[1], Chang-peng XIA[1]

1. School of Materials Science and Engineering, University of Jinan, Jinan 250022, China;
2. Jinan Chanyan Graphene Aluminum Material Technology Co., Ltd., Jinan 250031, China;
3. Dingmei New Material Technology Co., Ltd., Suzhou 215300, China

Received 27 November 2020; accepted 4 January 2022

Abstract: Gr/CuCr10 alloys with graphene contents of 0.1 wt.%, 0.3 wt.%, 0.5 wt.%, and 0.7 wt.% were prepared by a hot pressing sintering process. Compared with CuCr10 alloy, the relative density of CuCr10 composite with 0.3 wt.% addition of graphene remained constant, while the electrical conductivity increased from 62.2% (IACS) to 69.5% (IACS). The main reason for the increased electrical conductivity is that the addition of graphene leads to the size reduction of Cr phase and thus reduces the scattering of electrons. In addition, Brinell's hardness of 0.3 wt.% Gr/CuCr10 composite increased from HB 91.8 to HB 99.6 compared with that of CuCr10 alloy. The graphene was mainly distributed at the interface of Cu and Cr. A nano-$Cr_{23}C_6$ phase, which has been observed through HRTEM, is the main reason for the wettability enhancement at the interface of Cu and Cr, thus improving the hardness of the material.
Key words: graphene; CuCr alloy; vacuum hot pressing sintering; microstructure; electrical conductivity

1 Introduction

CuCr alloys have been widely applied as the electrical contact materials due to the outstanding high voltage stability, low current cut-off level, large current breaking capacity, and distinguished durability. As a result, CuCr alloy has become the dominant electrical contact material for medium voltage vacuum circuit breakers [1−3]. The increase of hardness is beneficial to enhancing the deformation resistance, voltage withstand level, and arc erosion resistance of CuCr alloy, and the electrical conductivity determines the service lives and application efficiency of the electrical contact devices. Therefore, the hardness and electrical conductivity are used as the main factors to evaluate the properties of CuCr alloys [4−6]. Previous studies have shown that the properties of CuCr contact alloys are highly related to the Cr-rich phase content, and the morphology of the Cr phase determines the properties of the alloys [7,8]. It was found that the Cr phase in the CuCr alloy mainly existed in a dendritic shape provided that it was prepared through conventional technologies, and this dendritic shape Cr phase has negative effects on the hardness and dielectric properties of the alloy [9−11]. As a result, it is necessary to align the microstructure of the Cr phase and enhance the electrical and mechanical properties of the CuCr alloys.

To reduce the size of the dendrite shape Cr phase in the CuCr system, 0.05 wt.% Ce was added in the CuCr15 alloy, and the diameter of the dendrite phase has been considerably reduced in an as-cast sample, leading to a significant improvement of the strength and slight increase of the electrical conductivity [12]. TIAN et al [13]

Corresponding author: Jin-feng LENG, Tel: +86-13954197005, E-mail: jfleng@126.com
DOI: 10.1016/S1003-6326(22)65868-0

revealed that, although the electrical conductivity was slightly sacrificed, 0.24 wt.% Zr addition to CuCr15 alloy was beneficial to forming fine CuZr grains which greatly inhibited the formation of eutectic Cr, and thus leading to the size reduction of Cr dendrite in an as-cast alloy. A similar result showed that 0.4 wt.% Zr addition to the CuCr10 alloy resulted in a smaller size of the Cr dendrite phase in an as-cast sample which significantly improved the strength but decreased the electrical conductivity [14]. It can be deduced that the addition of the third alloying element such as Ce, Ag, Co, or Si to CuCr alloy can refine the size of the Cr phase and improve the strength but reduce the electrical conductivity at the same time. As a result, it is necessary to find out a method to enhance the mechanical properties but not sacrifice the electrical conductivity of the alloys.

Graphene has an ultrahigh strength, excellent carrier mobility (15000 $cm^2/(V·s)$), and excellent thermal conductivity (5000 W/(m·K)), making it become a candidate for the reinforcement of metal matrix composites [15,16]. CHU et al [17] added a small amount of graphene and Cr to the Cu matrix, resulting in the formation of a small amount of Cr_7C_3 interface layer at the reduced graphene/CuCr interface, which was conducive to the transmission of electrons and loads. However, the research on graphene/CuCr (Gr/CuCr) composites was limited to a trace of Cr (≤1.0 wt.%) [18,19], and the CuCr alloys with high content Cr (≥5.0 wt.%) have not been investigated specifically.

In this work, Gr/CuCr10 composites were prepared by vacuum hot pressing sintering process. The effects of graphene content on the microstructure and properties of CuCr10 alloy were studied. Meanwhile, the corresponding interface products and interface structures were also investigated.

2 Experimental

Cu powder (≥99.00%, ~48 μm, Sinopharm Group), Cr powder (≥99.00%, ~13 μm, Xindu Alloy Co., Ltd.), and graphene were used as starting materials. The Cr powder and graphene powder were ball-milled in a planetary ball mill machine by using ethanol as an agent for 2 h with a speed of 150 r/m. The mass ratio of the stainless steel ball to the mixed powders was 10:1. The CuCr10 (the mass of copper and chromium was 90 and 10 g, respectively) and Gr/CuCr10 (The mass of copper is 90 g and the mass of chromium is 10 g; the graphene content is (0.1−0.7) wt.%) powders were loaded into a graphite die with a diameter of 20 mm and uniaxially pressed at room temperature with a pressure of 30 MPa and holded for 1 min and followed by vacuum hot pressing with a sintering temperature of 900 °C, a heating rate of 10 °C/min, an axial pressure of 30 MPa, and a soaking time of 2 h.

The hardness was measured using a Brovie optical durometer with a load of 613 N for 20 s on the freshly polished surface of CuCr10 and Gr/CuCr10 composites. The hardness of each sample was tested 10 times. The density of the material was measured and calculated by a drainage method. The resistance of arc erosion was characterized by the self refitted relay in the laboratory. The CuCr electrical contact material was made into a square sample with a side length of 10 mm and a thickness of 2 mm, and welded to the contact strip. The current of the arc erosion experiment was 80 A, the time of contact opening and closing was 4 s, and the total running time was 2 h. The conductivity of the samples was measured with a four-probe conductivity tester. The microstructures were characterized by a transmission electron microscope (JEM−2010 TEM) at 200 kV and a scanning electron microscope (QUANTA FEG 250).

3 Results and discussion

3.1 Microstructures of Gr/CuCr10 composites

Figure 1 shows the microstructure and element distribution of 0.5 wt.% Gr/CuCr10 composite. It can be seen that the Cr phases, with a size of 5−100 μm, are distributed in the copper matrix. Part of graphene is uniformly distributed within the Cu matrix with a rod or a plate shape. In addition, due to the uneven dispersion of graphene in the process of powder metallurgy, the graphene forms lumps and folds, resulting in an increase in thickness [20].

3.2 Interface structures of Gr/CuCr10 composites

Figure 2 shows the representative TEM images of the interface structure of Gr/CuCr10 composite. It displays an intimate interfacial adhesion between

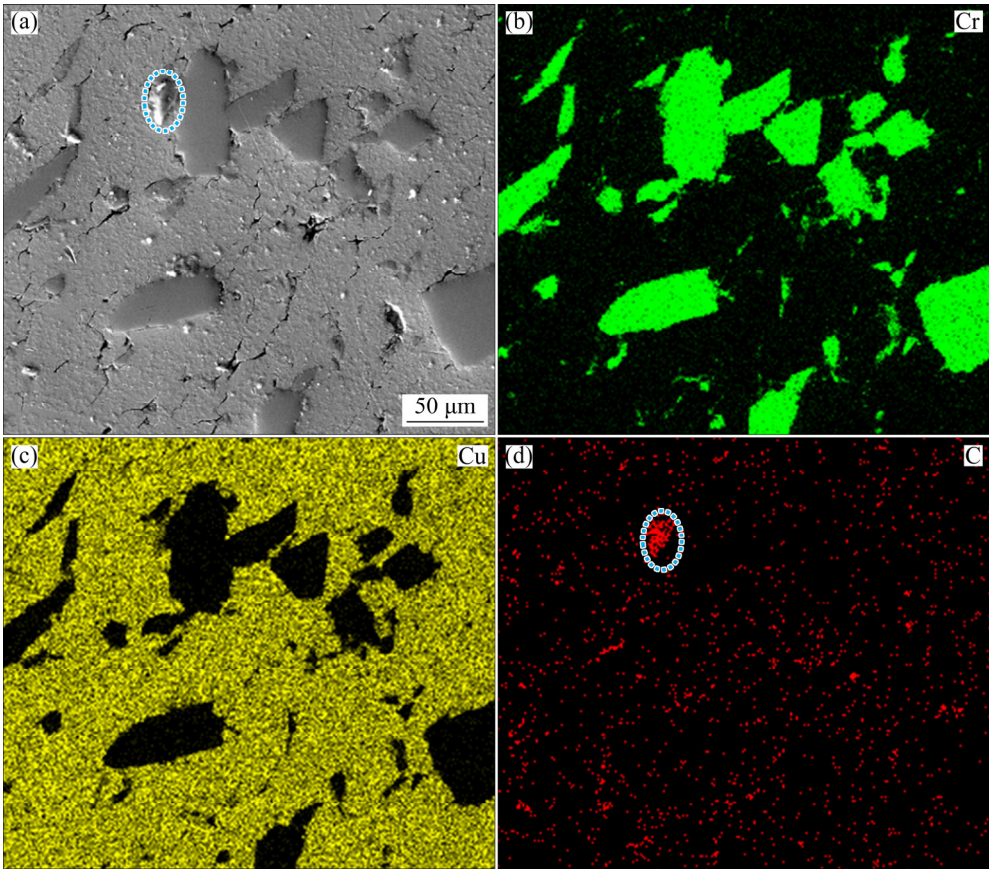

Fig. 1 Microstructure (a) and element distribution (b−d) of 0.5 wt.% Gr/CuCr10 composite

the graphene and the CuCr matrix without the presence of voids or cracks. To characterize the interfacial structure of the Gr/CuCr10 composites, the Fast Fourier Transform (FFT) and the Inverse Fast Fourier Transform (IFFT) techniques were applied to the HRTEM images. The HRTEM images show that there is a distinctive interface with a width of approximately 10 nm between the Cu matrix and the amorphous nano layer (AC) layer. The AC layer is a common amorphous layer at Cu/graphene interface, with a thickness of 10−40 nm. During the deformation process, the compaction and shear between the Cu and graphene particles cause the damage to the graphene, resulting in the formation of the AC layer during sintering. In the FFT image, the white box shows the $(0\bar{2}\,\bar{2})$, (422), and (400) diffraction spots of the $Cr_{23}C_6$ along the $[0\,\bar{1}1]$ zone axis, and the (022), (400), and (422) diffraction spots of $Cr_{23}C_6$ along the $[0\,\bar{1}1]$ zone axis (Figs. 2(d) and (i)). In the C−Cr system, there are three potential reactions [21,22]:

$$3Cr+2C=Cr_3C,\ \Delta G=-58857-22.34T \quad (1)$$

$$7Cr+3C=Cr_7C_3,\ \Delta G=-92067-41.5T \quad (2)$$

$$23Cr+6C=Cr_{23}C_6,\ \Delta G=-236331-86.2T \quad (3)$$

where ΔG is the Gibbs free energy change and T is the reaction temperature. When reaction temperature is 1173 K, the ΔG is −32.6, −43.4 and −135.2 kJ/mol for formation of Cr_3C_2, Cr_7C_3 and $Cr_{23}C_6$, respectively. Obviously, the ΔG of the formation of $Cr_{23}C_6$ is the lowest, so the compound between the Cu matrix and the AC layer can also be determined as $Cr_{23}C_6$. CHU et al [16] indicated that Cr_7C_3 phase was found at the interface between Cu matrix and AC layer rather than $Cr_{23}C_6$ phase due to the low content of Cr. However, the $Cr_{23}C_6$ phase is observed in this study, which is attributed to the sufficient amount of chromium addition. Due to the defects of graphene, AC layer is formed during the sintering process [23]. Then, Cr atoms diffuse to AC layer and react with active carbon atoms to form $Cr_{23}C_6$ phase.

3.3 Effect of Gr on CuCr microstructure

Figure 3 shows the metallographic structure of the Gr/CuCr10 composites with various grapheme contents, indicating that the Cr particles are homogeneously distributed in the Cu matrix. To

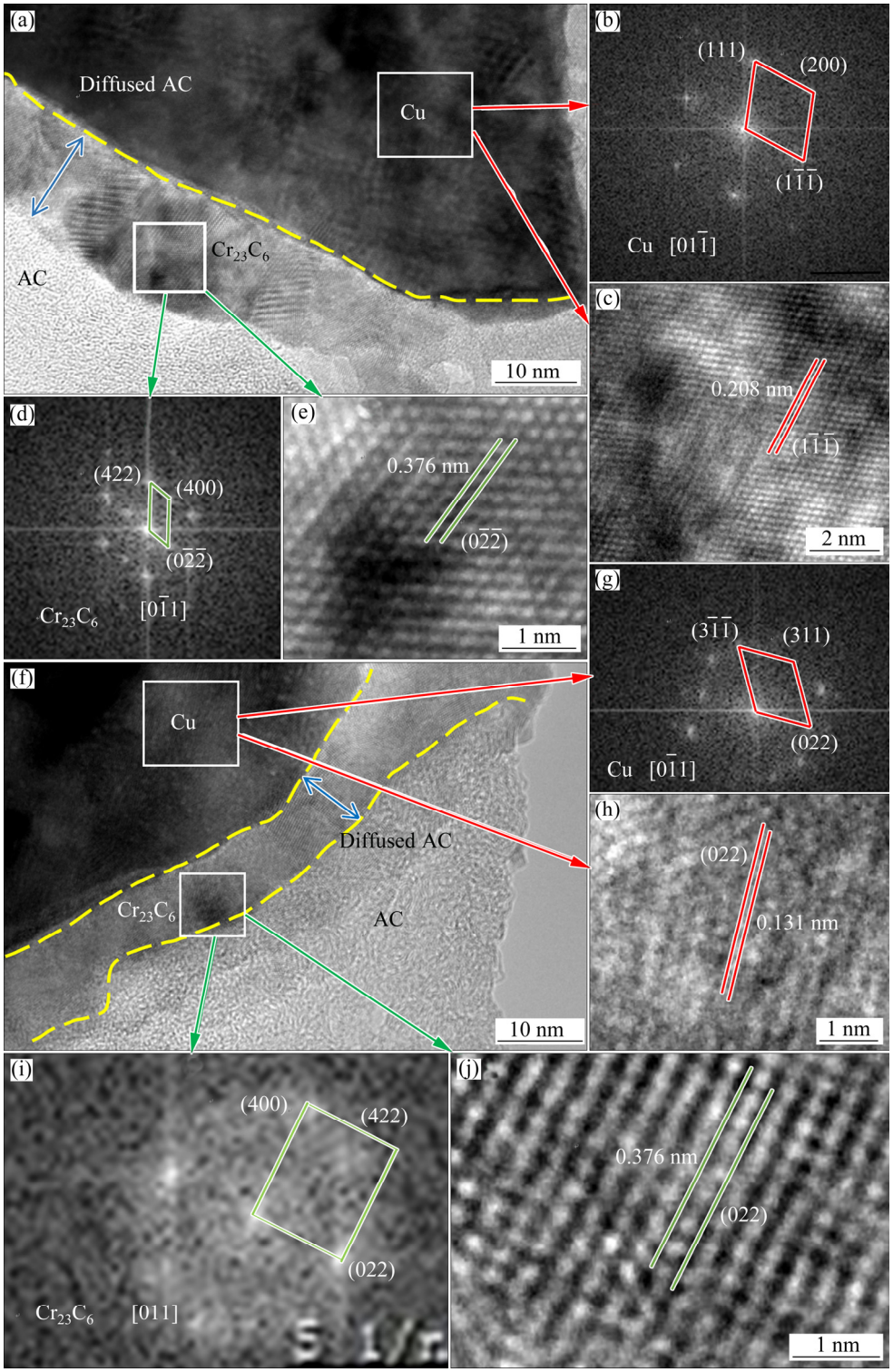

Fig. 2 HRTEM (a, f), FFT (b, d, g, i) and IFFT (c, e, h, j) images of 0.5 wt.% Gr/CuCr10 composite

quantitatively analyze the effect of graphene content on the size of the Cr particle, the particle sizes of 100 chromium phases in Gr/CuCr10 were counted and calculated to obtain the frequency distribution, as shown in Fig. 4. The results show that the Cr phase size decreases with the increase of graphene content when the graphene content is between 0 and 0.5 wt.%. When the graphene content is 0.5 wt.%, the average grain size of the Cr phase is 21.7 μm, 41.4% smaller than that of the CuCr10 alloy. When the amount of graphene is 0.7 wt.%, the particle size of Cr begins to increase

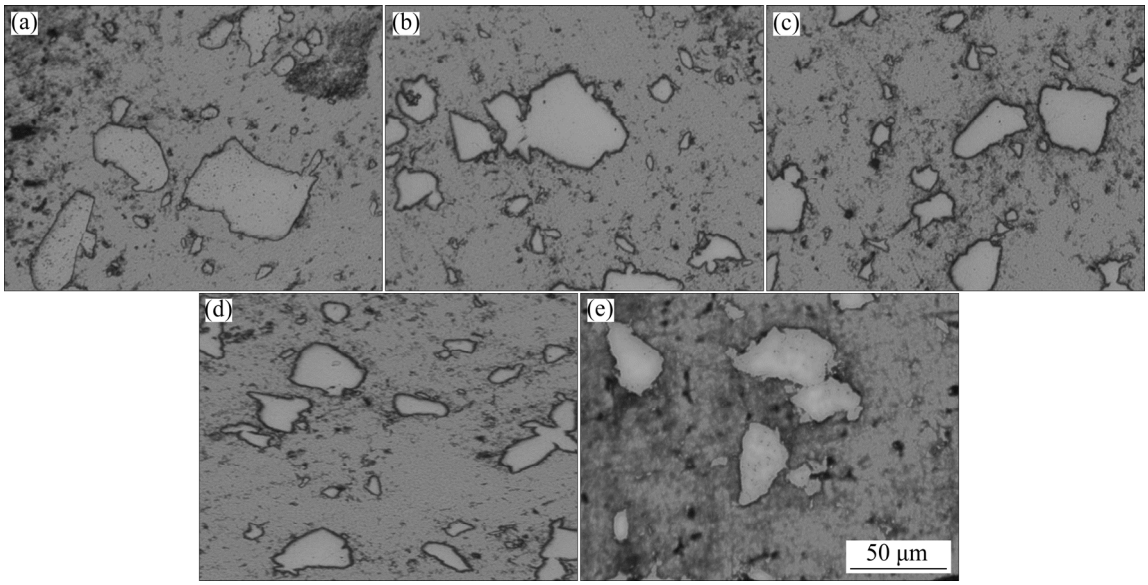

Fig. 3 Metallographic structures of Gr/CuCr10 composites: (a) 0 wt.% Gr; (b) 0.1 wt.% Gr; (c) 0.3 wt.% Gr; (d) 0.5 wt.% Gr; (e) 0.7 wt.% Gr

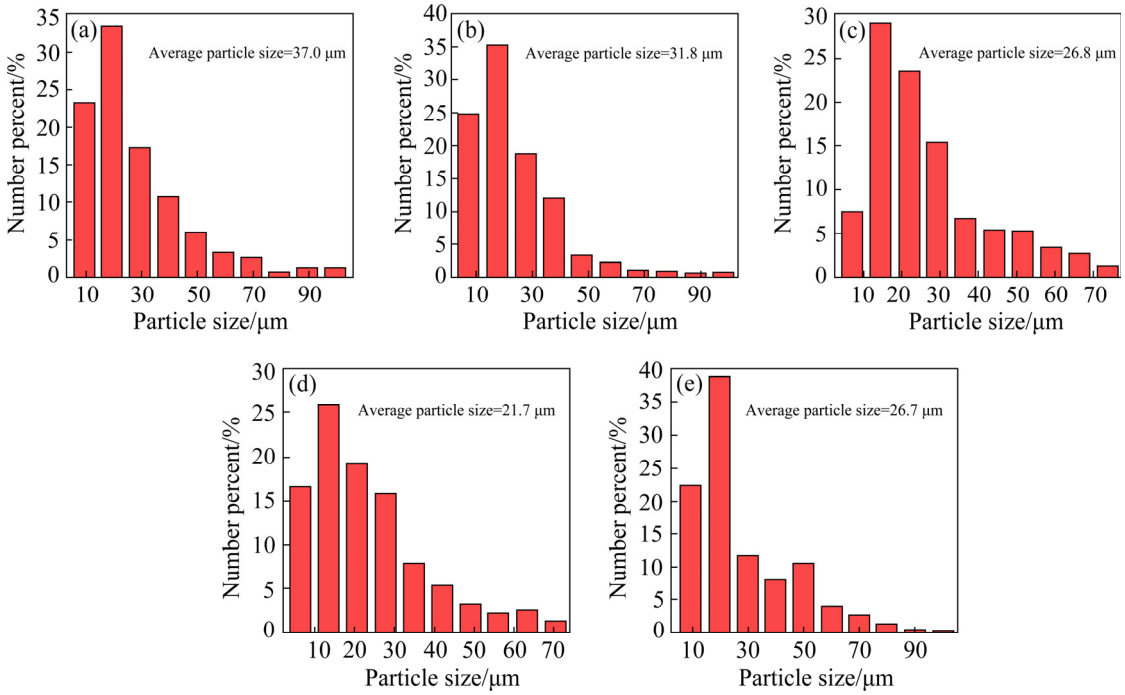

Fig. 4 Frequency distribution of Cr phase particle size in Gr/CuCr10 composites: (a) 0 wt.% Gr; (b) 0.1 wt.% Gr; (c) 0.3 wt.% Gr; (d) 0.5 wt.% Gr; (e) 0.7 wt.% Gr

again, but it is still smaller than that of the CuCr10. The effect of graphene on the refinement of the Cr phase is mainly reflected in the fact that a single or a few layers of Gr play an essential role in the interface, blocking the agglomeration of Cr grains during the sintering process. The graphene distributed around the Cr particles destroys the bonding force between the Cr grains and reduces the agglomeration of Cr.

Figure 5 shows the relative density of the Gr/CuCr10 composites with various graphene contents. As the content of graphene increases, the relative density of the Gr/CuCr10 shows a gradual dwindle trend. The relative densities of the 0.1 wt.% Gr/CuCr10 and the 0.3 wt.% Gr/CuCr10 are 97.3% and 97.2%, respectively, which are very close to the density of the CuCr10 (97.9%). When the content of the graphene changes from 0.5 wt.%

to 0.7 wt.%, the relative density of Gr/CuCr10 reduces significantly, and the relative density of 0.7 wt.% Gr/CuCr10 is 92.8%. Therefore, the addition of a small amount of graphene (≤0.3 wt.%) has slight effect on the density of Gr/CuCr10. When the content of the graphene is greater than 0.3 wt.%, the graphene will agglomerate together and become impurity phase in the matrix (insets in Figs. 5(a) and (b)), leading to a rapid increase of matrix defects, such as holes, and a decrease of the relative density of the prepared material. During the sintering process, severe agglomeration and weak fluidity of graphene hindered the plastic slip between particles, making it difficult for larger pores to be discharged under the pressure. At the same time, these defects also become a source of micro-cracks, resulting in reduced strength and fracture of the material.

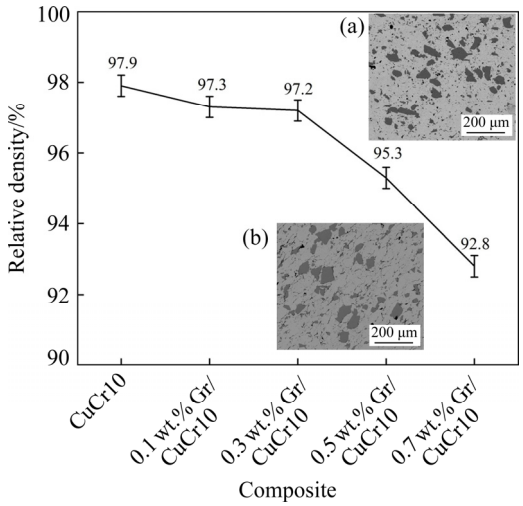

Fig. 5 Relative density of Gr/CuCr10 composites (Insets show agglomeration of graphene in 0.5 wt.% Gr/CuCr10 (a) and 0.7 wt.% Gr/CuCr10 (b))

3.4 Effect of Gr on CuCr10 properties

Figure 6 shows Brinell's hardness and conductivity curves of the Gr/CuCr10 composites with various graphene contents. When the content of the graphene is in the range of 0.1 wt.% to 0.5 wt.%, the hardness of the Gr/CuCr10 composite increases with the increase of the graphene content. When the content of graphene is 0.5 wt.%, the maximum value of hardness is HB 102.5, which is 11.7% higher than that of the CuCr10 alloy. When the content of the graphene increases to 0.7 wt.%, the hardness of the 0.7 wt.% Gr/CuCr10 decreases to HV 97.2. Due to the saturation of graphene content, a large number of graphene particles are distributed along the grain boundary, which reduces the bonding degree between matrix particles and decreases the relative density of materials, and finally negatively affects the continuous improvement of hardness. In addition, the graphene gathered at the grain boundary becomes the source of microcracks, thus forming small cracks and affecting the hardness of the material.

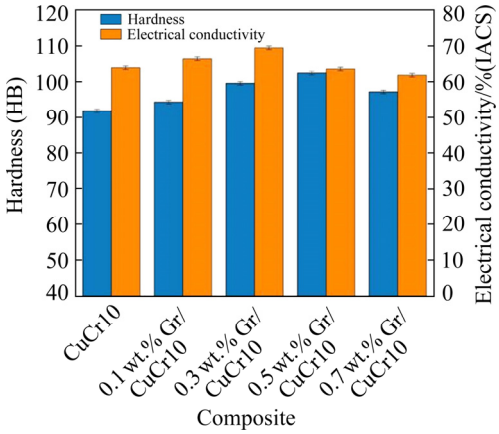

Fig. 6 Brinell's hardness and electrical conductivity of Gr/CuCr10 composites

$Cr_{23}C_6$ particle is observed at the interface between the graphene and the CuCr, which compensates for the low wettability of Cu and graphene. The graphene in the interface layer produces a load transfer effect, improving the hardness of the composite. The principle of load transfer of graphene in the interface layer is shown in Fig. 7. When the external pressure is applied on the surface of the graphene, the pressure load is transferred laterally through the discontinuous graphene interface layer, so the stress concentrated on the indenter can be effectively dispersed. Moreover, graphene has high elastic modulus, strength, and outstanding bearing capacity for external pressure, which greatly reduces the bearing stress of Cu. With an increase of the pressure, the load will be transferred down to the graphene layer, which reduces the shear stress at the interface, as shown by the arrows in Fig. 7. When the stress in the interface layer exceeds the yield limit, CuCr matrix will enter the plastic state, making the surface of the matrix plastic deform. The interface graphene plays the role of load transfer and improves the hardness of composites.

The electrical conductivity of the Gr/CuCr10 composite material reaches the optimal value of

69.5% (IACS) when the graphene content is 0.3 wt.%, which is increased by 8.6% compared to that of CuCr10. As the addition of graphene increases to 0.5 wt.%, the electrical conductivity of Gr/CuCr10 composites tends to decrease. The major reason for the decrease in the electrical conductivity of 0.5 wt.% Gr/CuCr composites is related to the holes of the composites. The holes increase the electron scattering ability and cause the drop in electrical conductivity.

The arc erosion resistance of the graphene-reinforced CuCr10 composites was realized by using a self-refitted relay method. Figures 8(a) and (d) show macroscopic morphologies of the CuCr10 alloy and the 0.5 wt.% Gr/CuCr10 composite after the arc erosion, respectively. The black particles can be observed in the central part, which were ash eroded by an electric arc. A shallow pit was formed in the corroded area, which is smaller than that in the non-corroded area. The number of black particles in the CuCr10 alloy is more than that of the 0.5 wt.% Gr/CuCr10 compositem, indicating that the arc erosion of the CuCr10 is severer than that of the Gr/CuCr10. In addition, by weighing the mass of the two materials before and after the arc erosion, the results indicate that the mass of the CuCr10 is 0.1896 g less than that of the samples before the arc erosion, and the mass of the 0.5 wt.% Gr/CuCr10 is reduced by 0.1761 g, as shown in Table 1. This indicates that the mass loss of the CuCr material with graphene is less than that of the non-graphene samples.

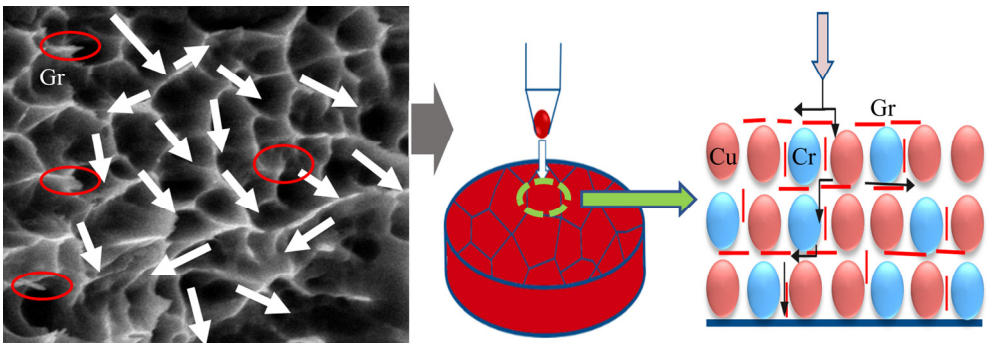

Fig. 7 Schematic diagram of load transfer principle of Gr/CuCr10 composite

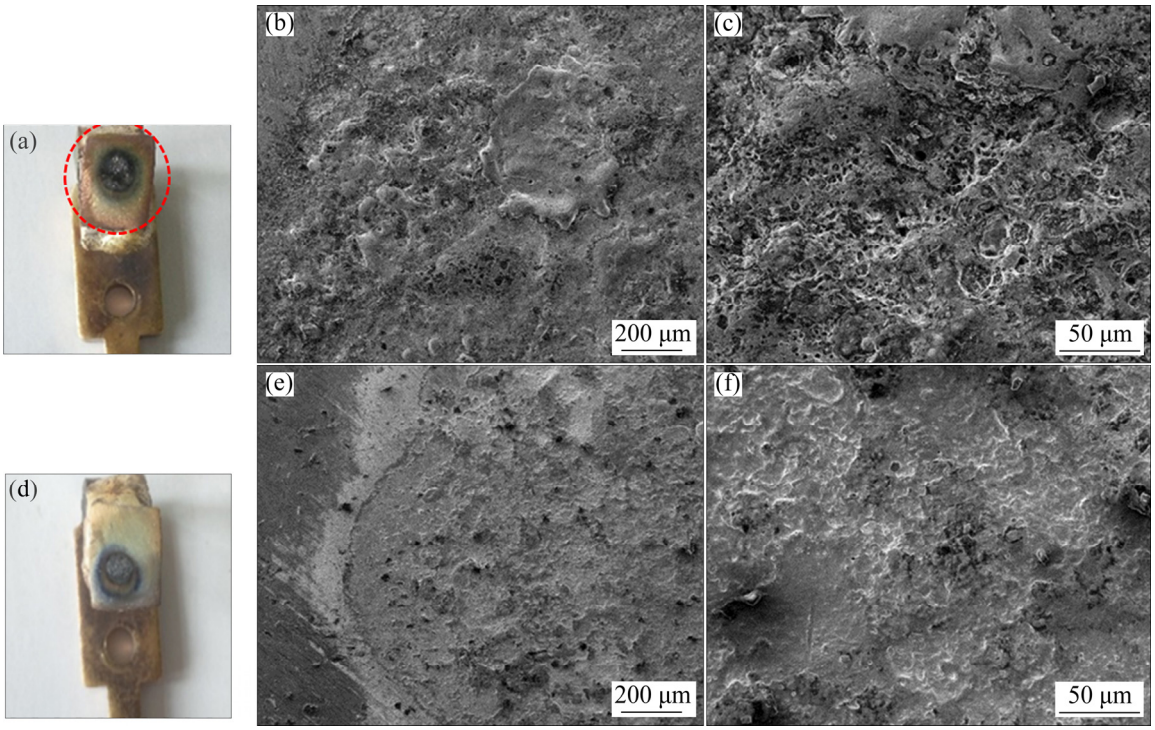

Fig. 8 Appearance after arc erosion (a, d) and SEM images (b, c, e, f) of samples: (a−c) CuCr10 alloy; (d−f) 0.5 wt.% Gr/CuCr10 composite

Table 1 Mass of CuCr10 and 0.5 wt.% Gr/CuCr10 before and after arc erosion

Material	Mass before erosion/g	Mass after erosion/g	Mass loss/g
CuCr10	15.1462	15.3358	0.1896
0.5 wt.% Gr/CuCr10	18.6936	18.5175	0.1761

It can be observed from Fig. 8(b) that the arc erosion surface of the samples is distinctive. Visible holes and impurities with a diameter of 50 μm can be observed, indicating that the welding point was deformed by the action of external force. And the inclusions, precipitates, grain boundaries, or sub-grain boundaries produce stress concentration and form microvoids. With the increase of the arc erosion cycling and the pressure applied on the samples, the area that has been eroded continues to be affected by both factors, so that the microvoids are continuously expanded until the material breaks and a plurality of micropores are left on the dimple of fracture. It can be seen from Figs. 8(e) and (f) that, the surface of the graphene-reinforced CuCr10 composite has no distinctive voids after the arc erosion test, the damage to the structure is less than that of the CuCr10 alloy, and the impurities and precipitates are less observable. Since the melting point of graphene is very high, CuCr10 alloy can be protected by the graphene during the process of arc erosion.

4 Conclusions

(1) A single layer or a few layers of graphene hinder the agglomeration and growth of Cr grains, leading to the refinement of the Cr phase. The average size of Cr particles decreases with adding graphene from 0.1 wt.% to 0.5 wt.%, and the average particle size of the 0.5 wt.% Gr/CuCr10 composite is 21.7 μm, which is 41.4% smaller than that of the CuCr10.

(2) A small amount of $Cr_{23}C_6$ phase is formed in situ at the Gr/CuCr interface, leading to the formation of a solid overall interface on Gr/CuCr10 composite material. The interfacial $Cr_{23}C_6$ layers/nanoparticles play a bridge role in firmly binding Gr on CuCr matrix, resulting in an overall strong interfacial bonding of Gr/CuCr10 composite.

(3) Graphene plays an essential role in the dispersion strengthening and second-phase strengthening for Gr/CuCr10 composites, and the properties of the Gr/CuCr10 composites are improved. When the content of graphene is 0.5 wt.%, the hardness of Gr/CuCr10 composite reaches the maximum value of HB 102.5; when the content of graphene is 0.3 wt.%, the electrical conductivity of the Gr/CuCr10 composite reaches the maximum value of 69.5% (IACS).

Acknowledgments

This work was financially supported by the National Natural Science Foundation of China (No. 51871111), Jinan Changan Graphene Aluminum Material Technology Co., Ltd., China, and the Dingmei New Material Technology Co., Ltd., China.

References

[1] ZHAO Qi, LEI Qian, GAN Xue-ping, ZHANG Long, ZHOU Ke-chao. Effects of the partially-unzipped carbon nanotubes on the microstructure and properties of CuCr matrix composites [J]. Diamond and Related Materials, 2020, 109: 108035.

[2] CHEN Yu-hong, REN Shu-bin, ZHAO Yang, QU Xuan-hui. Microstructure and properties of CuCr alloy manufactured by selective laser melting [J]. Journal of Alloys and Compounds, 2019, 786: 189−197.

[3] ZHANG Peng-chao, SHI Jie-fu, YU Ying-shui, SUN Jun-cai, LI Ting-ju. Effect of cryorolling on microstructure and property of high strength and high conductivity Cu−0.5wt.%Cr alloy [J]. Transactions of Nonferrous Metals Society of China, 2020, 30: 2472−2479.

[4] GARZÓN-MANJÓN A, CHRISTIANSEN L, KIRCH-LECHNER I, BREITBACH B, LIEBSCHER C H, SPRINGER H, DEHM G. Synthesis, microstructure, and hardness of rapidly solidified Cu−Cr alloys [J]. Journal of Alloys and Compounds, 2019, 794: 203−209.

[5] XIU Shi-xin, YANG Ren, XUE Jun, WANG Jin-xing, WANG Jia-yi. Microstructure and properties of CuCr contact materials with different Cr content [J]. Transactions of Nonferrous Metals Society of China, 2011, 21(S1): s389−s393.

[6] ZHANG Cheng-yu, WANG Ya-ping, YANG Zhi-mao, GUO Yong, DING Bing-jun. Microstructure and properties of vacuum induction melted CuCr25 alloys [J]. Journal of Alloys and Compounds, 2004, 366: 289−292.

[7] SHEN D P, ZHU Y J, YANG X, TONG W P. Investigation on the microstructure and properties of Cu−Cr alloy prepared by in-situ synthesis method [J]. Vacuum, 2018, 149: 207−213.

[8] WANG Jian, ZHANG Hong-tao, FU Hua-dong, XIE Jian-xin. Effect of Cr content on microstructure and properties of aged Cu−Cr−P alloys [J]. Transactions of Nonferrous Metals Society of China, 2021, 31: 232−242.

[9] ZHANG Cheng-yu, YANG Zhi-mao, WANG Ya-ping, DING Bing-jun, GUO Yong. Preparation of CuCr25 contact materials by vacuum induction melting [J]. Journal of

Materials Processing Technology, 2006, 178: 283−286.
[10] KLINSKI-WETZEL K V, KOWANDA C, HEILMAIER M, MUELLER F E H. The influence of microstructural features on the electrical conductivity of solid phase sintered CuCr composites [J]. Journal of Alloys and Compounds, 2015, 631: 237−247.
[11] ZHAO Lai-jun, LI Zhen-biao, SHI Kun-yu, HE Jun-jia, LI Hui-jie. Electrical properties of nanocrystalline CuCr25 contact material [J]. IEEE Transactions on Components, Packaging and Manufacturing Technology, 2013, 3(4): 625−632.
[12] LI Wen-you, LI Ya-ming, LI Wen-sheng, KONG Xiang-bo, WANG Hua. Microstructure and properties of deformed Cu−15Cr−Ce in-situ composites [J]. Chinese Journal of Nonferrous Metals, 2014, 24: 1518−1523. (in Chinese)
[13] TIAN Wei, BI Li-ming, MA Feng-cang, DU Jian-di. Effect of Zr on as-cast microstructure and properties of Cu−Cr alloy [J]. Vacuum, 2018, 149: 238−247.
[14] DENG Jian-qi, ZHANG Xiu-qing, SHANG Shu-zhen, LIU Fu, ZHAO Zu-xin, YE Yi-fu. Effect of Zr addition on the microstructure and properties of Cu−10Cr in situ composites [J]. Materials & Design, 2009, 30: 4444−4449.
[15] ZHAO R, AHKTAR M, ALRUQI A, DHARMASENA R, JASINSKI J B, THANTIRIGE R M, SUMANASEKERA G U. Electrical transport properties of graphene nanowalls grown at low temperature using plasma enhanced chemical vapor deposition [J]. Materials Research Express, 2017, 4(5): 055007.
[16] CHU Ke, LIU Ya-ping, WANG Jiang, GENG Zhong-rong, LI Yuan-bo. Oxygen plasma treatment for improving graphene distribution and mechanical properties of graphene/copper composites [J]. Materials Science and Engineering A, 2018, 735: 398−407.
[17] CHU Ke, WANG Fan, LI Yu-biao, WANG Xiao-hu, HUANG Da-jian, ZHANG Hu. Interface structure and strengthening behavior of graphene/CuCr composites [J]. Carbon, 2018, 133: 127−139.
[18] SI Xiao-yang, LI Mian, CHEN Fan-yan, EKLUND P, XUE Jian-ming, HUANG Feng, DU Shi-yu, HUANG Qing. Effect of carbide interlayers on the microstructure and properties of graphene-nanoplatelet-reinforced copper matrix composites [J]. Materials Science and Engineering A, 2017, 708: 311−318.
[19] CHU Ke, WANG Jing, LIU Ya-ping, LI Yuan-bo, JIA Cheng-chang, ZHANG Hu. Creating defects on graphene basal-plane toward interface optimization of graphene/CuCr composites [J]. Carbon, 2019, 143: 85−96.
[20] NAZEER F, MA Zhuang, GAO Li-hong, ABRAR S, MALIK A, KHAN M A, WANG Fu-chi, LI He-zhang. Higher mechanical and thermal properties of Cu−rGO composites [J]. Vacuum, 2020, 180: 109584.
[21] ANTHONYSAMY S, ANANTHASIVAN K, KALIAPPAN I, CHANDRAMOULI V, VASUDEVA RAO P R, MATHEWS C K, JACOB K T. Gibbs energies of formation of chromium carbides [J]. Metallurgical and Materials Transactions A, 1996, 27(7): 1919−1924.
[22] TENG L D, LU K G, AUNE R E, SEETHARAMAN S. Thermodynamic investigations of Cr_3C_2 and reassessment of the Cr−C system [J]. Metallurgical and Materials Transactions A, 2004, 35(12): 3673−3680.
[23] CHU Ke, WANG Fan, WANG Xiao-hu, LI Yu-biao, GENG Zhong-rong, HUANG Da-jian, ZHANG Hu. Interface design of graphene/copper composites by matrix alloying with titanium [J]. Materials & Design, 2018, 144: 290−303.

石墨烯对 Gr/CuCr10 复合材料显微组织和性能的影响

冷金凤[1]，周庆波[2]，李展之[3]，董云帆[1]，夏昌鹏[1]

1. 济南大学 材料科学与工程学院，济南 250022；
2. 济南产研烯金新材料科技有限公司，济南 250031；
3. 鼎镁新材料科技股份有限公司，苏州 215300

摘 要：采用热压烧结工艺制备石墨烯含量分别为 0.1%、0.3%、0.5%和 0.7% (质量分数)的 Gr/CuCr10 合金。与 CuCr10 合金相比，石墨烯添加量为 0.3%(质量分数)的 CuCr10 复合材料相对密度保持不变，而电导率从 62.2%(IACS)增加到 69.5%(IACS)。导电率增加的主要原因是石墨烯的加入导致 Cr 相尺寸减小，从而减少电子的散射。此外，与 CuCr10 合金相比，0.3%Gr/CuCr10(质量分数)复合材料的布氏硬度从 HB 91.8 增加到 HB 99.6。石墨烯主要分布在 Cu 和 Cr 的界面。通过 HRTEM 观察到的纳米 $Cr_{23}C_6$ 相是 Cu 和 Cr 界面润湿性增强的主要原因，从而提高了材料的硬度。

关键词：石墨烯；CuCr 合金；真空热压烧结；显微组织；电导率

(Edited by Wei-ping CHEN)